Shear and flexural deformations in flextegrity segmental beams inspired by Leonardo’s triangular masonry construction

PROCEEDINGS A

royalsocietypublishing.org/journal/rspa

Research

Check for updates

Article submitted to journal

**Subject Areas:**
structural engineering, applied mathematics, mechanics

**Keywords:**
flextegrity segmental beam, bending/shear deformation, nonlinear analysis, experimental measurements, Leonardo da Vinci

**Author for correspondence:**
Gianni Royer-Carfagni
e-mail: gianni.royer@unipr.it

# Shear and flexural deformations in flextegrity segmental beams inspired by Leonardo's triangular masonry construction

C. Boni[1] and G. Royer-Carfagni[1,2]

[1]Department of Engineering and Architecture, University of Parma, Parco Area delle Scienze 181/A, I-43124 Parma, Italy

[2]Construction Technologies Institute – Italian National Research Council (ITC-CNR), Via Lombardia 49, I-20098 San Giuliano Milanese, Milan, Italy

In *Tabula XCI verso* of Codex Atlanticus, Leonardo da Vinci presents an ingenious masonry structure composed of segments in the shape of inverted triangles. These are assembled by contact in a chain to obtain a lintel or jack arch, where they are pressed together by the thrust of the end constraints. Drawing inspiration from Leonardo's sketches, we show that, by connecting the segments in pair through elastic tendons, this system represents a new type of flextegrity beam. In a classical flextegrity, the contact surfaces of the segments are curved conjugate profiles, imposing a pure rolling motion along properly-designed pitch lines: the consequent elongation of the tendon dictates the constitutive response as a function of the relative rotation of the segments. Here the contact is through plane surfaces, so that the kinematics, besides the relative rotation, is characterized by segmental shearing. This system is theoretically analyzed and a continuum model is derived as the length of the segments becomes small. Comparisons with experiments on 3D-printed prototypes confirm the theoretical findings and highlight the possible competition between rotational and sliding types of deformation. Apart from the historical value, this type of construction can be used in innovative structures or metamaterials.

## 1. Introduction

Leonardo da Vinci was not only an outstanding artist, but also a master of natural philosophy and engineering



THE ROYAL SOCIETY PUBLISHING

science [1]. His contributions to geometry [2], fluid dynamics [3], friction [4], structural mechanics [5], and mechanism and machine theory [6] are worldwide recognized and appreciated. His brilliant intuitions can be re-visited, as has often been the case [7,8], in intriguing innovative applications.

The structural concept here discussed is inspired by the particular form of segmental masonry construction drawn in the *Tabula XCI verso* of the Codex Atlanticus [9], reproduced in Figure 1. Evidently, Leonardo aimed at an organized assembly of interlocked blocks. The structure below in the picture is composed of segments with stepped contact surfaces, which rule out their relative sliding in one direction (unilateral shear constraint). Observe, in passing, that although modern beam theory was not yet established in Leonardo's time, the shape of segmental interlocking is designed according to the sign of the shear diagram under self-weight. Our attention, however, focuses on the structure above. Here, each segment is composed of two flipped triangular portions, permanently bonded together; the segments are then assembled in unilateral contact. In Leonardo's notes[1] alongside the drawings, one can read on the first line «*I dua triangholi [h]anno a essere appicchati insieme e d'un pezzo*» (the two triangles must be stuck together and in one piece); and inside the triangular segment «*D'un pezzo i due triangoli*» (the two triangles in one piece). Possible applications as door lintel are mentioned in the second line: «*Quessto di sopra e quessto di sotto sono modi d'un archo, over chardinal d'usscio, da ffarllo di pezzi*» (this one above and this one below are ways of an arch, above door hinges, to be made of pieces).

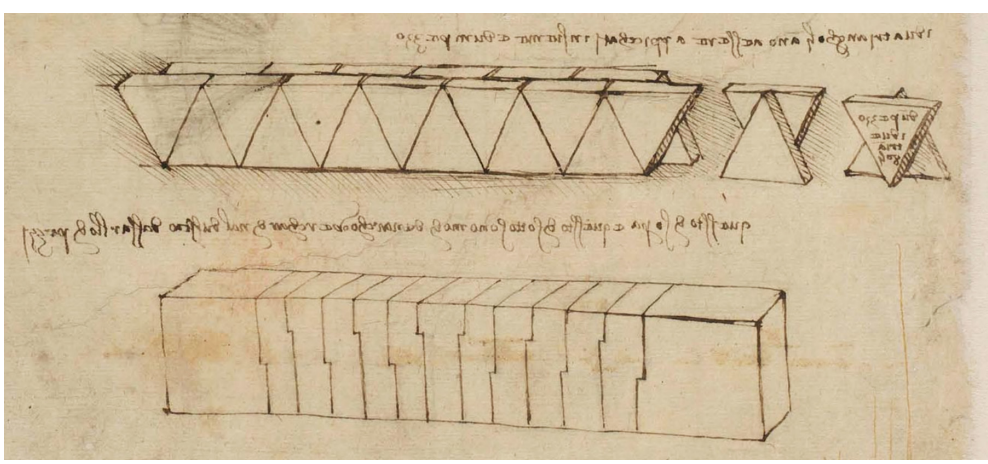

**Figure 1.** Drawing by Leonardo da Vinci reported in the *Tabula XCI verso* of the Codex Atlanticus [9]. Two possible ways to obtain a lintel or jack arch by means of a segmental masonry construction with interlocked blocks: triangular segments (above), and stepped contact surfaces (below).

Evidently, the proposed system was conceived as a masonry lintel or a jack arch with interlocked blocks, which shall be pressed together by the thrust provided by the end constraints. Here, we re-elaborate this concept, by imagining that the integrity of the system is provided by pre-tensioned elastic tendons, pairwise coupling the segments. In this configuration, the structural system can be counted in the category of *flextegrity*.

Flextegrity, originally named[2] *flexural tensegrity* [11], is a broad concept that can be defined in many forms [12–15]. In the fundamental setting, a flextegrity is essentially a segmental beam consisting of one chain of pierced segments in unilateral contact, held together by one prestressing

[1]Leonardo used to write from the right- to the left-hand side, so that the notes are mirrored with respect to normal writing. A commented transcription of the notes of Codex Atlanticus can be found in [10].

[2]The original name *flexural tensegrity* [11] was later shortened in *flextegrity* to avoid any possible confusion with the tensegrity structures by Buckminster Füller.

unbonded tendon passing through the segmental holes [11]. The main characteristic is that the contact surfaces are shaped such to achieve a *pure rolling motion* along the design (curved) pitch profiles. This can be obtained with conjugate profiles, such as the toothed profiles used in gears, as well as with other more elaborated shapes of the type considered in [11]. The relative rotation between any two consecutive segments, guided by the geometry of the contact surfaces, dictates the elongation of the tendons, which provides the main contribution to the strain energy of the system. In all cases, the pitch point (instantaneous center of rotation) is univocally determined by the relative rotation of the two consecutive segments.

On the contrary, in Leonardo's structure the contact surface is planar in the undeformed reference configuration: any pair of segments may relatively slide and rotate. The amount of sliding and rotation depends upon the shear force and the bending moment acting at the level of the segmental contact joints, as well as on the friction coefficient. This competition between sliding and rotation introduces additional variables in the kinematics associated with the structural problem, which requires an ad hoc treatment.

The flextegrity system inspired by Leonardo's drawings is here theoretically analyzed in Section 2, considering the combination of shear and bending deformation mechanisms. The case in which the size of the segments tends to zero while the segmental beam maintains the same length or, alternatively, the segmental size remains fixed whereas the beam length becomes much larger of it, provides the continuum limit for the mechanical model. Possible analogies with prestressed reinforced-concrete segmental beams are also discussed. Section 3 records the experiments on 3D-printed prototypes, organized as cantilevers or simply-supported beams, finding a good agreement with the theoretical predictions. The main properties of the structural system, together with hints for possible future developments, are summarized in the Conclusions.

## 2. The structural concept

The triangular structural concept inspired by Leonardo is here developed. The geometry of the segments is detailed, and the possible deformation mechanisms analyzed. Governing equations for the assembly are derived from energy minimization. The continuum limit of the mechanical model, as the ratio between the length of the beam and the length of the segments becomes very large, is also derived.

### (a) The segmental construction with triangular units

Each segment of the chain is composed by two portions, permanently stuck together. Both portions are identical equilateral triangles with a given thickness, flipped of 180° the one with respect to the other. Figure 2(a) reports a schematic view of one segment, with indication of the main dimensions. Circular fillets chamfer the vertices of the triangles, to achieve smoother movements when the segments are relatively displaced while remaining in contact, by decreasing stress concentrations. Different views of the corresponding 3D-printed segments are collected in Figure 2(b). These were built out of polylactide and the weight of each one is 0.132 N.

An assembled beam, made of 10 segments, is shown in Figure 2(c). Each segment is drilled crosswise at its centroid, and a wooden stick fits into the hole, protruding from the lateral surface of the segment: this serves to anchor rubber bands between each pair of consecutive segments (symmetrically placed bands for each pair), which keep them together. The wheels applied to the end segments simulate a roller constraint, to reproduce the condition of simple support. Since the elastic bands are forced in place, the segments result to be prestressed in the reference straight configuration.

The elastic bands were preliminary tested with a Galdabini Quasar 2.5 testing machine. The bands were connected to two hooks, fixed respectively to the upper and the lower crossbars of the testing machine. The clamping device reproduces the real condition on the structure, where the elastic bands are anchored to the wooden studs protruding from the lateral surface of the segments, which have the same radius as the hooks. The axial stiffness of the elastic ligament

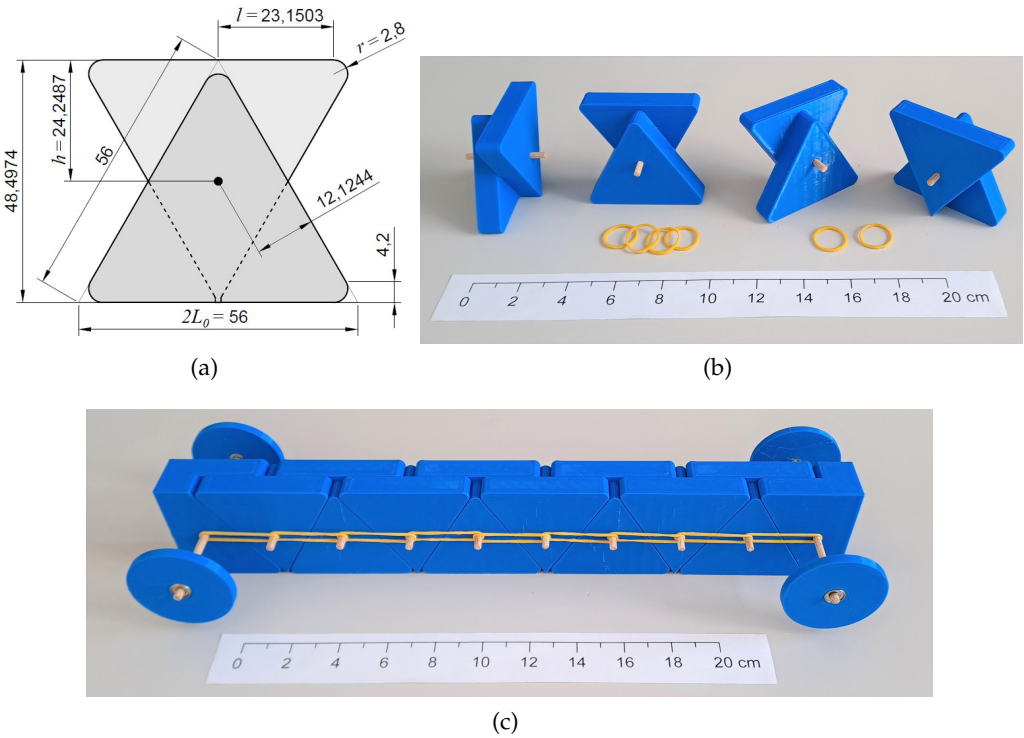


**Figure 2.** Details of the segments and their assembly in a beam. (a) Construction drawing of one segment with indication of main dimensions [mm]; (b) view of the 3D-printed segments and the (yellow) rubber bands; (c) assembled simply-supported beam composed by 10 segments, with end wheels to simulate roller constraints.

provided by *each one* of the elastic bands coupling two consecutive segments was measured to be equal to $k = 0.065\,\mathrm{N/mm}$. Taking into account the initial length of the band and the distance between the wooden studs in the reference configuration, the initial prestressing force transmitted by each elastic band between the consecutive segments was estimated to be equal to $N_0 = 0.585\,\mathrm{N}$.

## (b) Deformation mechanisms and governing equations

Let $n$ denote the number of segments forming the beam. Any two consecutive segments $i$ and $i+1$, with $i = 1 \ldots n-1$, are in unilateral contact and pressed together by the elastic bands. Their relative movement is described by the relative rotation $\Delta\varphi_i$, as schematized in Figure 3(a), and the relative sliding $\Delta v_i$, indicated in Figure 3(b), or a combination of sliding and rotation, according to the notation of Figure 3(c). We shall assume that $\Delta\varphi_i$ is positive if the segment on the right-hand side rotates clockwise with respect to the one on the left-hand side, and that $\Delta v_i$ is positive if the right-hand-side segment moves downwards with respect to the left-hand-side one. In all cases, the initial distance $L_0$ between the centroids of the segments increases to the actual value $L_i$, which is a function of $\Delta\varphi_i$ and/or $\Delta v_i$. This determines the elongation of the elastic bands $\Lambda_i = L_i - L_0$. Since the forces involved are small, the deformation of the bulk material forming the segments can be neglected. Hence, the elastic energy of the system is dictated by the elongation of the elastic bands only.

Figure 4(a) shows the elongation $\Lambda_i$ as a function of the variables $\Delta\varphi_i$ and $\Delta v_i$, indicated in Figure 3. It should be observed that the surface is not convex. A detail view of the surface plot for $\Delta v_i \geq 0$ and $\Delta\varphi_i \geq 0$ is reported in Figure 4(b), whereas the curves associated with the limit cases $\Delta v_i = 0$ and $\Delta\varphi_i = 0$ are shown in Figure 4(c). These curves represent the conditions of practical interest, since it has been observed that, in most cases, sliding and rotation do not

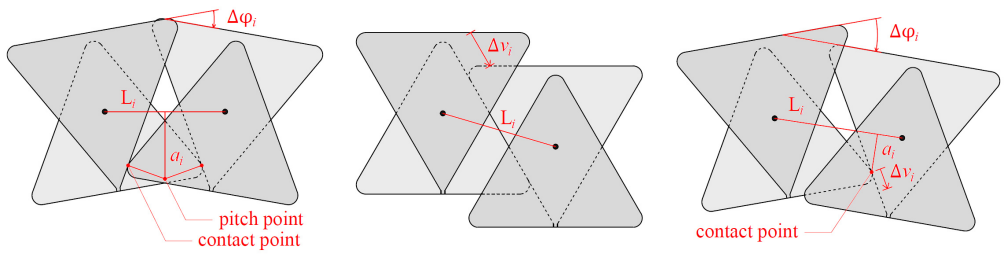


**Figure 3.** Deformation mechanisms of two consecutive segments: (a) pure rotation $\Delta\varphi_i$ (positive if clockwise) between the segments; (b) pure sliding $\Delta v_i$ (positive if downwards) between the segments; (c) combination of sliding and rotation. The length $a_i$ is the lever arm for the definition of the internal bending moment transmitted at the contact joint.

combine together, i.e., the deformation is characterized by either pure sliding or pure rotation at each contact joint, even if there can be both rotating and sliding joints within the same beam.

In particular, when $\Delta v_i = 0$ (pure rotation), for the geometry of Figure 2(a), one has

$$L_i = \cos\left(\frac{\pi}{6} - |\Delta\varphi_i|\right)\left[l + r\cot\left(\frac{\pi}{6} + \frac{|\Delta\varphi_i|}{2}\right)\right]\sec\left(\frac{\pi}{6} - \frac{|\Delta\varphi_i|}{2}\right) + 2h\sin\frac{|\Delta\varphi_i|}{2}\,. \tag{2.1}$$

For the case at hand, $l = 23.15\,\text{mm}$, $h = 24.25\,\text{mm}$, $r = 2.80\,\text{mm}$. Hence, by subtracting $L_0 = 28.00\,\text{mm}$, and, introducing a polynomial approximation, which is very accurate in the range $|\Delta\varphi_i| \le \pi/3$, one obtains

$$\Lambda_i = -9.360469\Delta{\varphi_i}^2 + 26.731615|\Delta\varphi_i|\,, \tag{2.2}$$

with $\Delta\varphi_i$ measured in radians. On the other hand, for the case of pure sliding ($\Delta\varphi_i = 0$), one has

$$L_i = \sqrt{\left(L_0 + |\Delta v_i|\cos\frac{\pi}{3}\right)^2 + \left(\Delta v_i \sin\frac{\pi}{3}\right)^2}\,. \tag{2.3}$$

For the case of combined sliding and rotation, one may assume that the two segments first relatively rotate one another and then slide. The resulting expression is quite lengthy, but using the polynomial approximation of (2.1), one obtains

$$\begin{aligned} L_i = \Bigg\{ &\left[(-9.36\Delta{\varphi_i}^2 + 26.73|\Delta\varphi_i| + 28.00)\right. \\ &\left. + |\Delta v_i|\cos\left(\frac{\pi}{3} + \frac{|\Delta\varphi_i|}{2}\right)\right]^2 + \left[\Delta v_i \sin\left(\frac{\pi}{3} + \frac{|\Delta\varphi_i|}{2}\right)\right]^2\Bigg\}^{\frac{1}{2}}. \end{aligned} \tag{2.4}$$

Neglecting the straining of the bulk material of which the segments are made, the increase $\Delta U$ of elastic energy, due to the elongation of the elastic bands, reads

$$\Delta U = N_0\left(\sum_{i=1}^{n-1}\alpha_i\Lambda_i\right) + \frac{1}{2}k\left(\sum_{i=1}^{n-1}\alpha_i{\Lambda_i}^2\right), \tag{2.5}$$

being $\alpha_i$ the number of elastic bands at the $i-$th joint ($\alpha_i = 2$, for $i = 1\ldots 9$, in Figure 2(c)).

In case of conservative forces such as gravitational loads, the work $\Delta W$ of external actions can be calculated according to the scheme of Figure 5. Starting from the reference configuration of straight horizontal beam under null external actions, each pair of consecutive segments relatively displaces in the vertical direction of the quantity $\Delta y_i$ (positive if the second segment relatively moves downwards), and one has

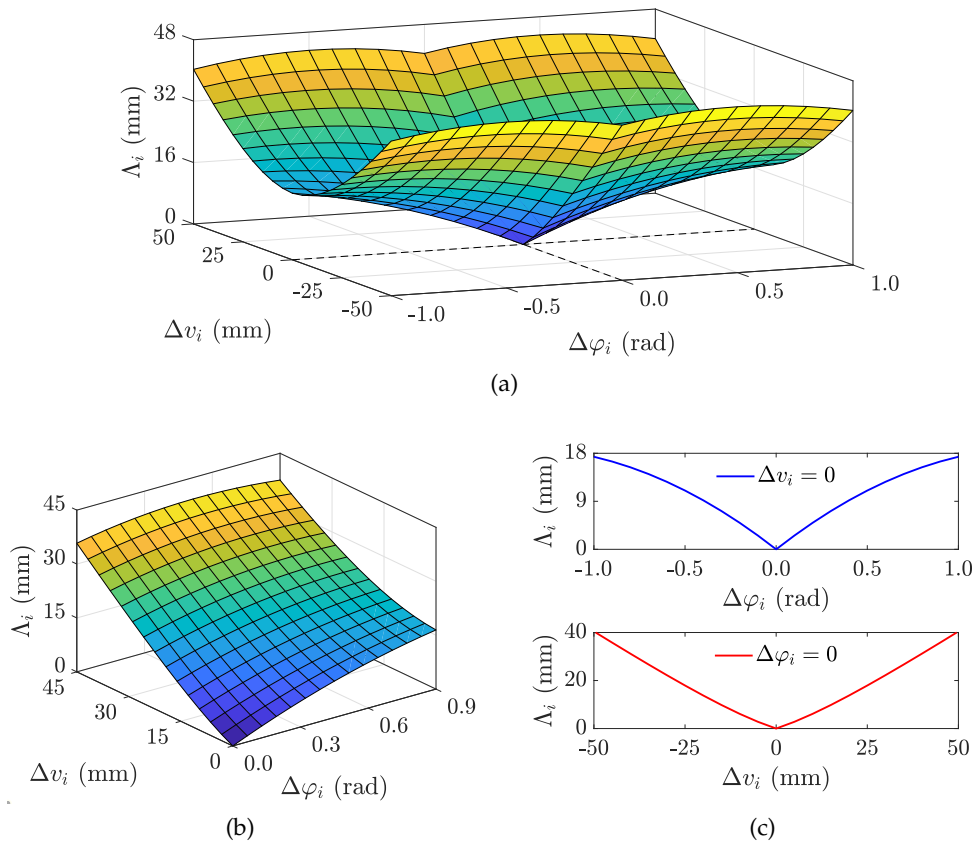


**Figure 4.** Elongation $\Lambda_i$ of the elastic bands at each joint $i$, when adjacent segments undergo the relative rotation $\Delta\varphi_i$ and the relative sliding $\Delta v_i$. (a) Surface plot of $\Lambda_i$ and (b) detail for $\Delta v_i \geq 0$ and $\Delta\varphi_i \geq 0$; (c) limit curves for $\Delta v_i = 0$ and $\Delta\varphi_i = 0$.

$$\Delta W = \sum_{i=1}^{n} P_i \left( \sum_{j=0}^{i-1} \Delta y_j \right) , \tag{2.6}$$

where $\Delta y_0$ is the displacement of the first segment (for the case of Figure 5, where the first segment is clamped, one has $\Delta y_0 = 0$). Obviously, $\Delta y_i$ is a function of the Lagrangian variables $\Delta v_i$ and $\Delta\varphi_i$. The corresponding expressions are quite lengthy, but can be calculated from elementary geometry.

We assume that frictional forces are negligible: this hypothesis will be discussed in the next Section 3 and corroborated by experimental findings. Therefore, the actual values of $\Delta\varphi_i$ and $\Delta v_i$ can be obtained from energy minimization, that is

$$\Delta U - \Delta W = \min , \tag{2.7}$$

under the boundary conditions associated with the end constraints.

From (2.7), a set of equilibrium equations is obtained. In particular, when the contact is pointwise, as in the cases indicated in Figures 3(a) and 3(c), one can demonstrate [11] that the internal bending moment transmitted at the contact joint is $M_i = \alpha_i N_i a_i$, where $N_i = N_0 + k\Lambda_i$ is the actual axial force transmitted by each elastic band bonding the joint and $a_i$ represents the lever arm, indicated in the same figures. According to the sign convention of Figure 3, the bending moment, and correspondingly $a_i$, is positive if the extrados of the beam is under tensile stress, and viceversa. It is possible to verify, from geometric considerations [13] or following the variational

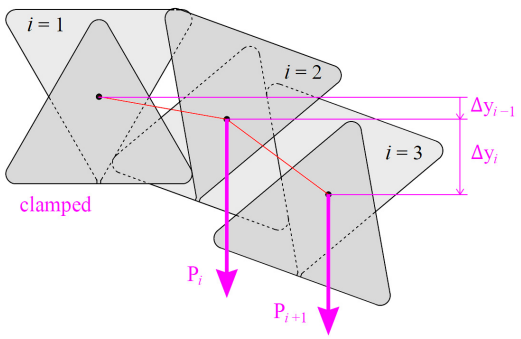


**Figure 5.** Schematic representation of the deformation of the segmental beam. Here, the beam is a cantilever composed of three segments: segment $i=1$ is clamped and the loads $P_i$ and $P_{i+1}$ $(i=2)$ are applied at the centroid of the remaining segments; the work-conjugate displacements of these loads are $\Delta y_{i-1}$ and $\Delta y_{i-1}+\Delta y_i$, respectively.

arguments of [11], that $a_i = \mathrm{d}\Lambda_i/\mathrm{d}\Delta\varphi_i$. When the deformation involves only shear sliding, as in Figure 3(b), the contact surface is a plane and the bending moment cannot be determined from purely geometric considerations because the contact point is not predetermined.

In the examples that will considered in Section 3, the variational problem (2.7) shall be directly solved by using the minimization algorithm `FindMinimum` available in Wolfram Mathematica®.

## (c) The continuum limit

The continuum limit corresponds to the case in which the ratio between the size of the segments and the length of the beam goes to zero. One can associate this limit to a condition in which the number $n$ of segments becomes engineeringly large. This condition can be achieved when, keeping fixed the length of the beam, the size of the segments becomes very small.

For simplicity, consider a linearized kinematics under the hypothesis of small displacements. Also assume that the small fillet at the vertices of the triangles, indicated in Figure 2(a), is vanishing ($r \to 0$), so that $l = L_0$. Hence, one obtains from (2.1) that the elongation of the elastic bands due only to rotation, as in the case of Figure 3(a), reads

$$\Lambda_i \simeq \left(L_0 \sec\frac{\pi}{6}\right)|\Delta\varphi_i| = \frac{2\,L_0}{\sqrt{3}}|\Delta\varphi_i|\,, \tag{2.8}$$

which is accurate as long as $|\Delta\varphi_i| \ll 1$.

Since the lever arm $a_i$ in Figure 3(a) coincides with the first derivative of $\Lambda_i$ with respect to $\Delta\varphi_i$, then $|a_i| \simeq 2\,L_0/\sqrt{3}$ is constant. Therefore, considering that in a linearized theory the stress increase in the pre-tensioned bonding bands can be neglected, the bending moment at the joints is $M_i \simeq \alpha_i N_0 a_i$ and one deduces that the size of the segments cannot be reduced below a certain value. In fact, in the limit $L_0 \to 0$, an infinite initial prestress $N_0$ would be needed to provided a finite value of the bending moment $M_i$ at the joint.

An interesting observation indeed is that shear deformation mechanisms are ruled out in a beam of very small (vanishing) height, for which a very high (infinite) prestress $N_0$ is needed to provide flexural capacity. Therefore, this would activate a very high (infinite) resistance to sliding in case of friction, but no-sliding occurs also in the limit case of vanishing frictional angle. In fact, the first order contribution to the strain energy at each joint would be $2N_0L_0\alpha_i|\Delta\varphi_i|/\sqrt{3}$ for the rotation $\Delta\varphi_i$, and $N_0\alpha_i|\Delta v_i|/2$ for the slide $\Delta v_i$. When $L_0 \to 0$, one has $N_0 \to \infty$, so that the product $N_0L_0$ can remain finite: whereas the rotational contribution to the energy remains finite as well, on the other hand, the contribution due to sliding would become unboundedly large. Hence, it must be $\Delta v_i = 0$. This finding suggests that in slender beams the rotational contribution is the main source of deformation.

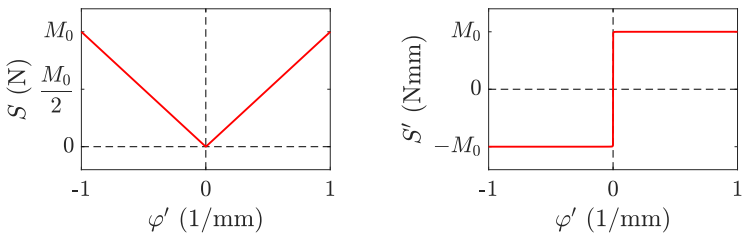


**Figure 6.** Continuum limit under the hypothesis of small displacements. Graphs of the strain-energy density $S(\varphi') = M_0\,|\varphi'|$ and its first derivative $S'(\varphi') = M_0\,\varphi'/|\varphi'|$, corresponding to the moment-curvature relationship.

Since $|a_i|$ is constant, when $\alpha_i = \text{const.} = \alpha$, a third remarkable conclusion is that $M_i$ is also constant and takes the value $|M_i| = 2\alpha N_0\, L_0/\sqrt{3} := M_0$.

When the segments, coupled by the $i-$th joint, only rotate one another, the relative vertical displacement $\Delta y_i$, positive if downwards, between their centroids reads

$$\Delta y_i = \Big(L_0 + \Lambda_i\Big)\sin\frac{\Delta\varphi_i}{2}\cos\sum_{j=0}^{i-1}\Delta\varphi_j + \Big(L_0 + \Lambda_i\Big)\cos\frac{\Delta\varphi_i}{2}\sin\sum_{j=0}^{i-1}\Delta\varphi_j\,, \tag{2.9}$$

where $\Delta\varphi_0$ is the rotation of the first segment.

In the continuum limit, we shall assume $L_0 \to 0$ and $N_0 \to \infty$, so that the product $N_0 L_0$ tends to a definite limit. Introduced the abscissa $s$ along the centroidal line of the beam, such that it is represented by $0 \le s \le \ell$, we shall call $L_0$ as $ds$ and define the rotation $\varphi(s)$ such that, at the $i-$th joint identified by $s = s_i$, the difference quotient $\Delta\varphi_i/L_0$ becomes the curvature $\varphi'(s_i)$. Moreover, we will introduce the displacement function $y(s)$ such that $\Delta y_i/L_0$ can be replaced by $y'(s_i)$.

After having expanded the sine and cosine functions in Taylor series, neglecting terms of order higher than one in $\Delta\varphi_i$ and substituting summations with integrals, one obtains from (2.9) that

$$y'(s_i) = \int_0^{s_i}\varphi'(\bar{s})\,\mathrm{d}\bar{s} = \varphi(s_i) - \varphi(0)\,. \tag{2.10}$$

Moreover, in the case in which $\alpha_i = \text{const.} = \alpha$, denoting the limit value $N_0 L_0$ as $M_0\sqrt{3}/(2\alpha)$, one obtains from (2.8) that

$$\sum_{i=0}^{n} N_0\alpha_i\Lambda_i = \frac{2}{\sqrt{3}}\alpha N_0 L_0\left(\sum_{i=0}^{n}\left|\frac{\Delta\varphi_i}{L_0}L_0\right|\right) \simeq M_0\int_0^{\ell}|\varphi'(s)|\,\mathrm{d}s\,. \tag{2.11}$$

To make the calculation explicit, consider the simplest case of a cantilever, such that the clamped end is at $s = 0$ (hence $\varphi(0) = 0$), and a concentrated force $P$ is applied at the tip $s = \ell$. From (2.10) and (2.11), the increase of strain energy and the work of the external load can be respectively written as

$$\Delta U = \int_0^{\ell} M_0|\varphi'(s)|\,\mathrm{d}s = \int_0^{\ell} S\left(\varphi'(s)\right)\,\mathrm{d}s\,, \tag{2.12a}$$

$$\Delta W = P\int_0^{\ell} y'(s)\,\mathrm{d}s = P\int_0^{\ell}\varphi(s)\,\mathrm{d}s\,, \tag{2.12b}$$

where $S(\varphi') = M_0\,|\varphi'|$ represents the strain energy density. The zeroing of the first variation of the energy functional (2.7) corresponds to the condition

$$M_0\int_0^{\ell}\frac{\varphi'(s)}{|\varphi'(s)|}\delta\varphi'(s)\,\mathrm{d}s - P\int_0^{\ell}\delta\varphi(s)\,\mathrm{d}s = 0\,. \tag{2.13}$$

Figure 6 reports the graphs of the strain energy density and its first derivative, i.e., the function $S'(\varphi') = M_0\,\varphi'/|\varphi'|$, which corresponds to the moment-curvature relationship. It is clear that the

response is rigid-plastic. The curvature is zero until the bending moment reaches the limit $\pm M_0$: at this stage, the curvature may grow unboundedly in the same verse of the bending moment, so to produce positive work.

The flexural response of beams whose moment-curvature relationship presents horizontal asymptotes $\pm M_0$ as the curvature tends to $\pm\infty$ (corresponding to oblique asymptotes for the strain energy density) was discussed in [16] from a variational point of view. Considering the limit behavior of the energy functional on sequences converging to singular functions, it was shown that the linear growth at infinity of the strain energy density is not sufficient to bind the curvature field: infinite curvatures may occur at points of the beam while the energy remains finite. Such singularities are represented by Dirac's masses for the curvature concentrated at isolated points, which are interpreted as localized rotations, similar-in-type to those corresponding to the formation of plastic hinges in the engineering theory of elastic-plastic beams. An application to elastic perfectly-plastic beams with various cross sections was then presented in [17].

The condition defined in Figure 6 represents a particular case of the general theory of [16], to which the reader is referred for the details: now the beam is rigid-plastic rather then elastic-plastic. When the bending moment can be calculated from sole statics (statically determined structure), the solution can be easily determined. The curvature is zero as long as the bending moment is, in absolute value, less than $M_0$; a plastic hinge, where the curvature concentrates (finite rotation) develops at the point where the bending moment reaches first the value $\pm M_0$.

In conclusion, the geometry of the joints with interlocked triangles provides, in the continuum limit in which the size of the triangles becomes engineeringly very small, a rigid-plastic moment-curvature constitutive law. This case, of mainly theoretical interest, may nonetheless indicate a trend for structural behavior. The difficulty of a passage to the limit lies in the fact that the structure is composed of equilateral triangles, and therefore the size of the segments cannot be reduced without also reducing the height of the beam. Therefore, the case of main practical interest is the one in which the beam is composed of a finite number of segments.

**Remark.** *An analogy is often evoked between flextegrities and prestressed reinforced-concrete segmental beams. The fact that the structure inspired by Leonardo's drawings exhibits both bending and shear deformation mechanisms, strengthens the search for such a comparison, but the two structural systems are fundamentally different.*

*In concrete beams, the segments are kept in contact by prestressed cables or bars, housed in tubular sheaths, possibly filled with cement mortar after the cables have been tensioned. In the serviceability limit state, there is usually no sliding due to shear (this is inhibited by the roughness of the contact surfaces and the possible presence of shear keys), nor joint opening due to bending. A smooth deflection is dictated by the straining of the concrete matrix. In the ultimate limit state, the steel yields, and large concentrated rotations may occur between the segments, while shear slip remains restrained by frictional contact, reliefs on the contact surfaces, as well as by the dowel action of the steel cables.*

*On the contrary, in the flextegrity structure, the bond provided by the elastic bands is mild. The structure is designed to undergo large segmental rotations also in the serviceability limit state. The response remains elastic (and reversible) even if the contact joints significantly slide and/or rotate. Since the system of pre-stress is "external", there is no dowel action from the tying elastic bands. The deflection of the flextegrity is mainly governed by the stretching of the elastic bands, since the segments are much stiffer than them. Even more important, the reciprocal sliding of the segments causes a longitudinal expansion due to the inclination of the contact surfaces, which does not occur in segmental concrete beams, where the sliding, if at all, shall occur on vertical planes.*

*Nevertheless, there are some analogies. The flextegrity inspired by Leonardo shows the transition from sliding deformation mechanism to rotation deformation mechanism as the beam becomes slender. This is in agreement with the behavior of reinforced-concrete beams, whose failure mode passes from shear to bending as the height of the beam is reduced. Moreover, we have demonstrated that, in the continuum limit, our model produces a rigid-plastic constitutive behavior. This evokes the formation of plastic hinges in reinforced-concrete beams. The possible formation of inclined fractures in the concrete, where the shear*

*action is predominant, can lead to slip deformations which recall those on the 60° inclined joint surfaces of Leonardo's flextegrity. However, in this case, friction and other tying effects, due to e.g. the dowel action of the steel bars, should be taken into account.*

## 3. Experiments

Beams made with the 3D-printed segments shown in Figure 2 were tested under the action of self-weight and concentrated loads. The deflection measured on the prototypes was compared with the results obtainable from the model presented in Section 2(b), to corroborate the theory.

The model overlooks the effects of friction. This certainly represents an ideal condition, but it can be approximately verified when estimating the equilibrium configurations under static loads. In our experiments, the 3D-printed prototypes were gently shaken during the gradual application of the loads, so as to annihilate the effect of parasitic friction at the joints and reach a condition as close as possible to the ideal one, in which external forces are balanced by internal elastic reactions.

### (a) Cantilever beams

A cantilever beam composed of four segments was tested first. Any two consecutive segments were coupled by two elastic bands, so that $\alpha_i = 2$ in (2.5), for $i = 1 \dots 3$. The structure was placed horizontally on a rigid support and clamped at one of the segments in order to obtain a cantilever beam. More in detail, three cases were analyzed, which differ in the number of overhanging segments from the constrained segments: one, two or three overhanging segments, as respectively shown in Figures 7(a), 7(b) and 7(c); according to Figure 5, we label the clamped segment in Figure 7 with $i = 1$. The self-weight (0.132 N per segment) and a tip load, represented by a hanging weight, are applied. After the application of the hanging weight, the structure was gently shaken, in order to annihilate the effect of parasitic friction at the joints.

For the case of Figure 7(a), the more convenient deformation mechanism is that of pure sliding, following the scheme of Figure 3(b). For varying hanging weight, the measured deflections at the tip, represented by $\Delta y_1$, according to the notation of Figure 5, are shown in Figure 8(a) with black dots (the size of the dots includes the errors in terms of load measurement; the horizonal bars indicate the uncertainties in measuring the deflection); the continuous blue curve corresponds to

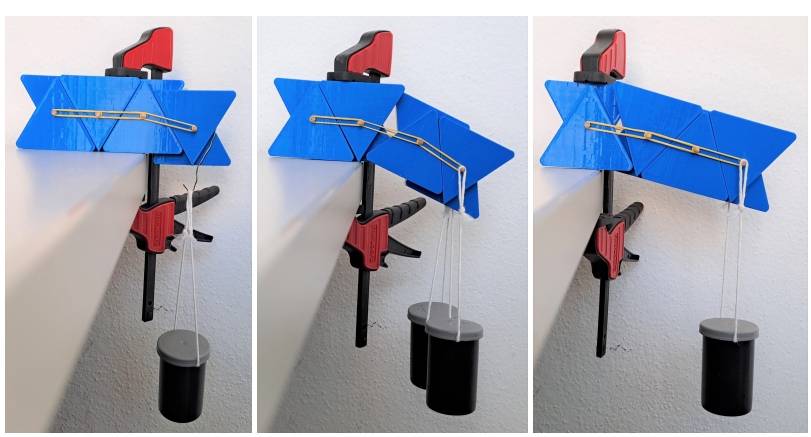

(a) (b) (c)

**Figure 7.** Tested cantilever beams subjected to self-weight and tip loads. Structure with (a) one, (b) two and (c) three overhanging segments.

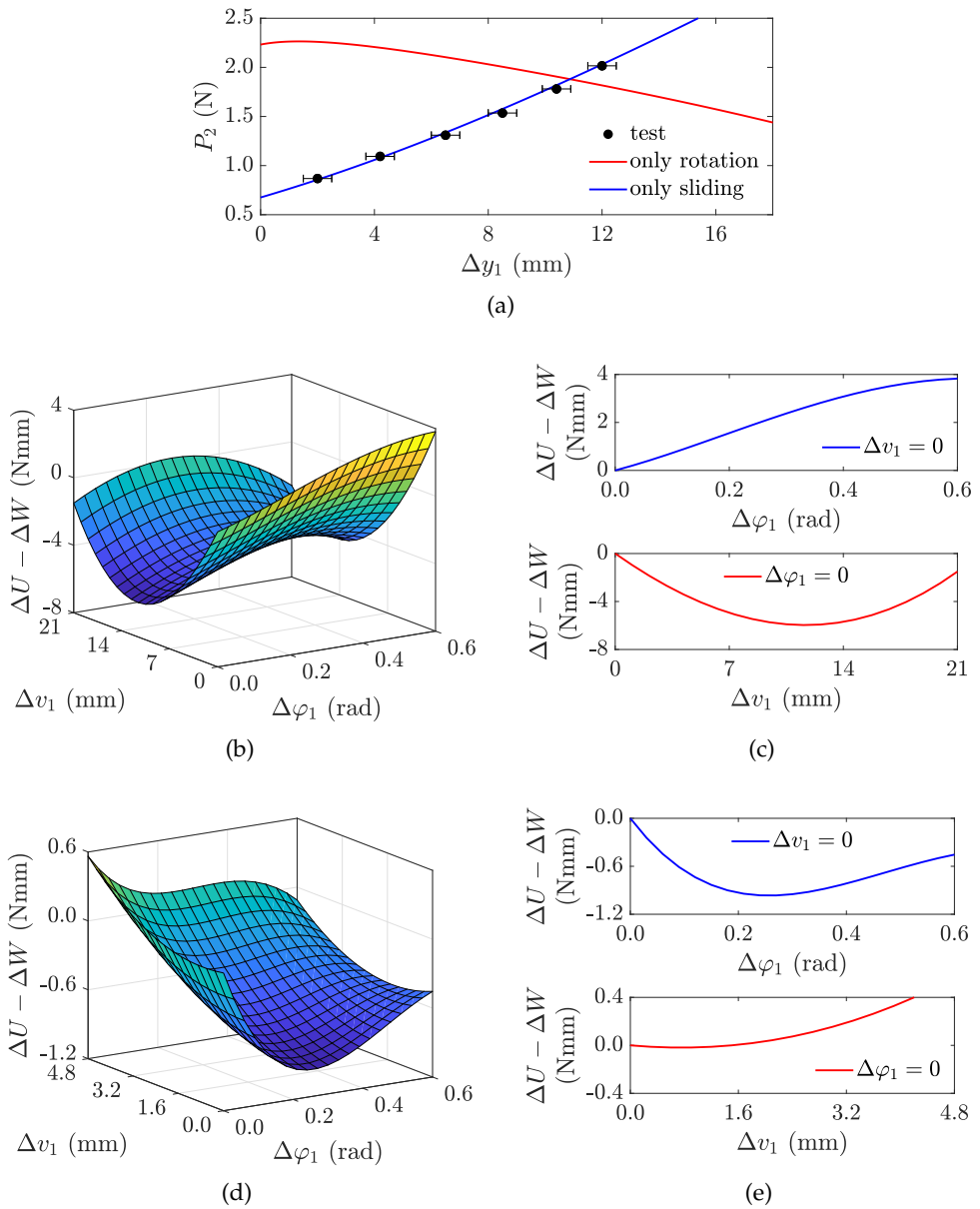


**Figure 8.** Test results and energy scenario. Cantilever with one overhanging segment (one joint): (a) load $P_2$ on the second segment from the clamped one and corresponding deflection $\Delta y_1$; experimental points (dots) and theoretical curves for pure sliding (blue) and pure rotation (red); (b) energy $\Delta U - \Delta W$ as a function of the rotation $\Delta\varphi_1$ and of the sliding $\Delta v_1$ for $P_2 = 1.781$ N; (c) detail of curves corresponding to the sections $\Delta v_1 = 0$ and $\Delta\varphi_1 = 0$. Cantilever with three overhanging segments and three joints: (d) energy plot as a function of $\Delta\varphi_1$ and $\Delta v_1$ at the joint next to the clamp and (e) curves at $\Delta v_1 = 0$ and $\Delta\varphi_1 = 0$ for $P_2 = P_3 = 0.132$ N and $P_4 = 0.467$ N.

the estimate from the model. For the sake of comparison, the same chart reports the red curve, corresponding to the equilibrium states for a deformation mechanism of pure rotation, of the type indicated in Figure 3(a). It is clear that the experimental points well overlap with the blue curve, confirming the sliding nature of the deformation mechanism; the red curve (rotation mechanism) cannot be attained because it would correspond to higher values of the applied load. This finding is confirmed by the plot of the total energy $\Delta U - \Delta W$, represented in Figure 8(b) as a function

**Table 1.** Deflection of the cantilever beam under self-weight and tip load: comparison between theoretical predictions and experimental measurements.

| | 2 joints - tip load $= 0.746\,\mathrm{N}$ | | 3 joints - tip load $= 0.335\,\mathrm{N}$ | |
|---|---|---|---|---|
| | experiment | model | experiment | model |
| $\Delta\varphi_1$ | $22.0 \pm 0.5$ deg | 22.9183 deg | $15.0 \pm 0.5$ deg | 14.7031 deg |
| $\Delta\varphi_2$ | $0.0 \pm 0.5$ deg | 0.0000 deg | $0.0 \pm 0.5$ deg | 0.0000 deg |
| $\Delta\varphi_3$ | — | — | $0.0 \pm 0.5$ deg | 0.0000 deg |
| $\Delta v_1$ | $3.0 \pm 0.2$ mm | 3.4366 mm | $0.0 \pm 0.2$ mm | 0.0000 mm |
| $\Delta v_2$ | $4.0 \pm 0.2$ mm | 4.0511 mm | $0.0 \pm 0.2$ mm | 0.0000 mm |
| $\Delta v_3$ | — | — | $0.0 \pm 0.2$ mm | 0.0000 mm |

of the Lagrangian variables $\Delta\varphi_1$ and $\Delta v_1$; Figure 8(c) reports a detail of the curves obtained at $\Delta v_1 = 0$ and $\Delta\varphi_1 = 0$. When the total load on the overhanging segment is $P_2 = 1.781\,\mathrm{N}$ (self-weight + hanging weight), the energy is minimized when $\Delta\varphi_1 = 0$ and $\Delta v_1 \simeq 10\,\mathrm{mm}$.

For the case of Figure 7(b), with two overhanging segments and two joints, the deformation is that of pure sliding for the second joint, while the first joint exhibits a combined of sliding and rotation, as in Figure 3(c), when the tip hanging weight is 0.746 N. This is the condition that minimizes the total energy for the model, which is now confirmed by the tests. A quantitative comparison between theory and experiments is reported in Table 1, for the case of tip load equal to $0.746\,\mathrm{N}$ (total loads on the segments are $P_2 = 0.132\,\mathrm{N}$ and $P_3 = 0.132 + 0.746 = 0.878\,\mathrm{N}$). There is a small difference in terms of $\Delta v_1$ but, considering the 3D printing tolerances and the action of parasitic friction, neglected in the model, the accuracy is reputed good.

As bending becomes dominant over shear, the deformation mechanism becomes that of Figure 3(a), i.e., pure rotation. This is evidenced by the slender cantilever of Figure 7(c), with three overhanging segments and three joints. In this case, the rotation is localized at the first joint, while the other two neither rotate nor slide. Figures 8(d) and 8(e) respectively report the plots of the total energy $\Delta U - \Delta W$ as a function of $\Delta\varphi_1$ and $\Delta v_1$, as well as the curves $\Delta v_1 = 0$ and $\Delta\varphi_1 = 0$, for a tip hanging weight equal to $0.335\,\mathrm{N}$: the minimum is at $\Delta v_1 = 0$. The comparison between the model and the experimental results is shown in Table 1 for the same tip weight of $0.335\,\mathrm{N}$ (total loads on the segments are $P_2 = P_3 = 0.132\,\mathrm{N}$ and $P_4 = 0.132 + 0.335 = 0.467\,\mathrm{N}$). In this case, the results from the tests are in perfect agreement with the experiments. The better accuracy with respect to the case with two joints may be attributed to the fact that, in a pure rotation mechanism, the frictional parasitic forces are certainly much smaller than in the case of sliding.

## (b) Simply-supported beams

A second experiment was conducted on a simply-supported beam, as reported in Figure 9. The beam is now composed of 10 segments, of the size indicated in Figure 2(a). The rollers at the extremities are realized by means of a shaft passing through segments $i = 1$ and $i = 10$ at the centroid and connected to wheels, as shown in Figure 2(c).

The beam was placed horizontally in the gravity field with the wheels engaged in a horizontal track, and a tandem load was applied at midspan. Two cases were considered, corresponding to two elastic bands per joint ($\alpha_i = 2$, for $i = 1 \dots 9$) and to four elastic bands per joint ($\alpha_i = 4$, for $i = 1 \dots 9$). Therefore, differently from the previous tests on cantilevers, where the number of overhanging segments was modified, we are now varying the stiffness of the joints for a fixed construction of the beam. The deflections of the beam in the two aforementioned configurations are respectively represented in Figures 9(a) and 9(b).

Table 2 compares the experimental findings with the prediction from the model in terms of the midspan deflection of the beam centerline under self-weight (0.132 N per segment) and external

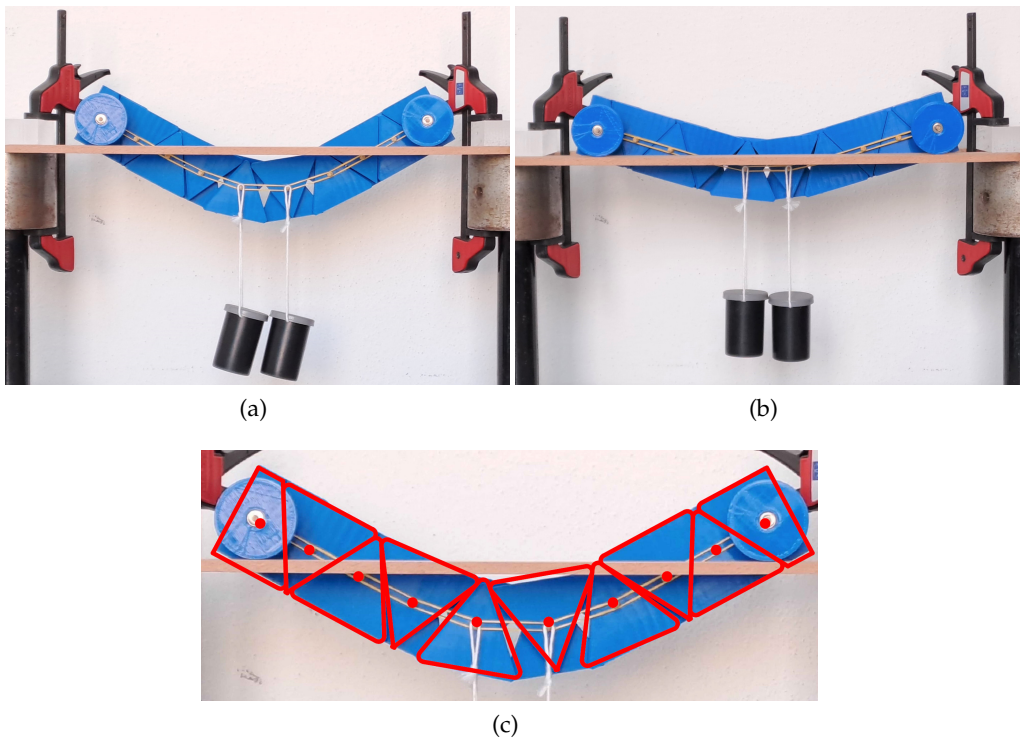

**Figure 9.** Simply-supported segmental beams subjected to a tandem load at midspan and self-weight. Cases with (a) two and (b) four elastic bands per joint, pairwise coupling the segments. Figure (c) juxtaposes the deflection of case (a) with the deformation predicted by the model (red solid line).

tandem loads: the accuracy of model is very good. As expected for this slender beam, for which bending is dominant over shear, the segments relatively rotate rather than slide. More in detail, the model correctly predicts the experimental finding that only the joints at the center of the beam (third to seventh joint) rotate, whereas the ones at the extremities remain tight.This result is not surprising, because a slender beam approximates the limit condition of continuous beams, discussed in Section 2(c), characterized by a rigid-plastic bending response. In the tested beams, only those joints where the bending moment reaches a threshold value will rotate, while the others remain closed.

The comparison between the deflection of the prototype of Figure 9(a) and the deformation predicted by the the model is displayed in Figure 9(c). The red lines and red dots, respectively representing the contours of the segments and their centroids, overlap well with the photograph. The slight deviations may be attributed, on the one hand, to the distortion introduced in the photograph by the camera wide angle, and, on the other hand, to a residual parasitic friction between the rollers and the track and between the contact surfaces at the joints, not considered in the model. In any case, the good comparison in Figure 9(c) confirms that these effects are of secondary importance.

## 4. Conclusions

A beam composed of triangular-shaped segments, inspired by Leonardo's drawings reported in Codex Atlanticus, has been theoretically analyzed, prototyped and tested. Originally conceived as a masonry jack arch, it may represent a new class of flextegrity structures for which the segments, instead of being joined together by the lateral thrust provided by the end restraints, are connected in pairs by elastic bands. The main difference with respect to the flextegrity beams so far proposed

**Table 2.** Deflection of the simply-supported beam under self-weight and midspan load: comparison between theoretical predictions and experimental measurements.

| | sagitta | | tandem load at midspan |
|---|---|---|---|
| | experiment | model | |
| 2 elastic bands per joint | $49 \pm 1$ mm | 49.3016 mm | $2 \times 0.098$ N |
| 4 elastic bands per joint | $27 \pm 1$ mm | 28.9877 mm | $2 \times 0.441$ N |

is that the segments can not only rotate but also relatively slide one another, thus enriching the deformation kinematics.

A model has been proposed under the assumption that the segments are rigid and that the contact friction is negligible. When the ratio between the length of the beam and the size of the segments goes to infinity, a continuous characterization has been obtained. Sliding has been found to occur in short beams, for which shear is dominant over bending; as the number of segments increases, the rotation mechanism takes over and becomes the only one possible in the continuous limit, which results to be governed by a rigid-plastic moment-curvature relationship. Experiments on 3D-printed cantilevers and simply-supported beams have confirmed the theoretical predictions.

Leonardo's segmental construction suggests a possible division of the two dimensional space into a homogeneous assemblage of equal similarly-oriented non-chiral cells, arranged in two layers of elementary geometric figures (equilateral triangles), pairwise coupled in the out-of-plane direction. Under the hypothesis that the cells are kept in contact by elastic bonds, the deformation mechanisms, here discussed for the simpler one-dimensional beam-like assembly, are represented by the combination of rotations and sliding of each cell with respect to the neighboring ones. This represents perhaps the simplest example of structured membranes obtained through the elastic connection of platelets with Voronoi-type tiling, characterized by the permanent coupling "in pairs" of tiles belonging to two adjacent layers. Hierarchical micro-architectures of this type can inspire innovative metamaterials, for which the tactics of rearrangement of the units under imposed actions is dictated by their elementary character, shape and orientation and the geometry of the contacts. The resulting properties, which may be tailor-designed through non-regular tessellations, are yet to be understood and appreciated.

## Declarations

**Data accessibility.** The Mathematica notebook that have been used to calculate the response of the cantilver beam with 2 joints (2joints.nb) and the Stereolithography file for the 3D-printing of segments (segment.stl) are provided in the electronic supplementary material.

**Authors' contributions.** C.B.: conceptualization, methodology, formal analysis, investigation, writing – original draft, writing – review and editing; G.R.-C.: conceptualization, analysis, methodology, supervision, writing – original draft, writing – review and editing. All authors gave final approval for publication and agreed to be held accountable for the work performed therein.

**Conflict of interest declaration.** There are no competing interests to declare.

**Funding.** This research did not receive any specific grant from funding agencies in the public, commercial, or not-for-profit sectors.

## References

1. Lieb JW. 1921 Leonardo da Vinci-Natural philosopher and engineer. *Journal of the Franklin Institute* **191**, 767–806.
2. Bokowski J, Wills JM. 2022 Regular Leonardo polyhedra: Mathematics and art. *The Art of Discrete and Applied Mathematics* **5**, 3–13.

3. Colagrossi A, Marrone S, Colagrossi P, Le Touzé D. 2021 Da Vinci's observation of turbulence: A French-Italian study aiming at numerically reproducing the physics behind one of his drawings, 500 years later. *Physics of Fluids* **33**, 115122.
4. Hutchings IM. 2016 Leonardo da Vinci's studies of friction. *Wear* **360**, 51–66.
5. Roelofs R. 2008 Two-and three-dimensional constructions based on Leonardo grids. *Nexus Network Journal: Leonardo da Vinci: Architecture and Mathematics* pp. 17–26.
6. Bucolo M, Buscarino A, Famoso C, Fortuna L, Gagliano S. 2020 Automation of the Leonardo da Vinci machines. *Machines* **8**, 53.
7. Fonseca AF, Galvao DS. 2021 Graphene-based nanoscale version of da Vinci's reciprocal structures. *Computational Materials Science* **187**, 110105.
8. Prete AC. 2022 Revolutionary Flight Vehicle Based on Leonardo Da Vinci Aerial Screw: A Paradigm Shift in VTOL Technology. Master's thesis University of Maryland, College Park.
9. da Vinci L. 1478–1518 Codex Atlanticus. Original handwritten manuscript at the Veneranda Biblioteca Ambrosiana in Milan, digitalized version available online at https://www.codex-atlanticus.it.
10. Marinoni A. 1976–1980 *Leonardo da Vinci: Codice Atlantico: trascrizione diplomatica e critica di Augusto Marinoni*. Firenze: Giunti-Barbera.
11. Boni C, Silvestri M, Royer-Carfagni G. 2020 Flexural tensegrity of segmental beams. *Proceedings of the Royal Society A* **476**, 20200062.
12. Boni C, Royer-Carfagni G. 2021a A nonlocal elastica inspired by flexural tensegrity. *International Journal of Engineering Science* **158**, 103421.
13. Boni C, Royer-Carfagni G. 2021b Equilibrium of bi-stable flexural-tensegrity segmental beams. *Journal of the Mechanics and Physics of Solids* **152**, 104411.
14. Boni C, Reis PM, Royer-Carfagni G. 2022 Flexural-tensegrity snapping tails for bio-inspired propulsion in fluids. *Extreme Mechanics Letters* **56**, 101853.
15. Boni C, Royer-Carfagni G. 2023 Flextegrity simple cubic lattices. *Proceedings of the Royal Society A* **479**, 20220637.
16. Royer-Carfagni G. 2001 Can a moment-curvature relationship describe the flexion of softening beams?. *European Journal of Mechanics, A/Solids* **20**, 253–276.
17. Royer-Carfagni G, Buratti G. 2007 Plastic hinges as phase transitions in strain softening beams. *Journal of Mechanics of Materials and Structures* **2**, 1677–1699.